Reaction Paths of Iron Oxidation and Hydrolysis in Horse Spleen and Recombinant Human Ferritins†

Xiaoke Yang,‡ Yu Chen-Barrett,‡ Paolo Arosio,§ and N. Dennis Chasteen*,‡

Department of Chemistry, University of New Hampshire, Durham, New Hampshire 03824, and DIBIT, Institute San Raffaele, Via Olgettina 58, 20232, Milano, Italy

Received December 19, 1997; Revised Manuscript Received March 16, 1998

ABSTRACT: UV−visible spectroscopy, electrode oximetry, and pH stat were used to study Fe(II) oxidation and hydrolysis in horse spleen ferritin (HoSF) and recombinant human H-chain and L-chain ferritins (HuHF and HuLF). Appropriate test reactions and electrode responses were measured, establishing the reliability of oxygen electrode/pH stat for kinetics studies of iron uptake by ferritin. Stoichiometric ratios, Fe(II)/O_2 and H^+/Fe(II), and rates of oxygen uptake and proton production were simultaneously measured as a function of iron loading of the protein. The data show a clear distinction between the diiron ferroxidase site and mineral surface catalyzed oxidation of Fe(II). The oxidation/hydrolysis reaction attributed to the ferroxidase site has been determined for the first time and is given by $2Fe^{2+} + O_2 + 3H_2O \rightarrow [Fe_2O(OH)_2]^{2+} + H_2O_2 + 2H^+$ where $[Fe_2O(OH)_2]^{2+}$ represents the hydrolyzed dinuclear iron(III) center postulated to be a μ-oxo-bridged species from UV spectrometric titration data and absorption band maxima. The transfer of iron from the ferroxidase site to the mineral core has been now established to be $[Fe_2O(OH)_2]^{2+} + H_2O \rightarrow 2FeOOH_{(core)} + 2H^+$. Regeneration of protein ferroxidase activity with time is observed for both HoSF and HuHF, consistent with their having enzymatic properties, and is facilitated by higher pH (7.0) and temperature (37 °C) and by the presence of L-subunit and is complete within 10 min. In accord with previous studies, the mineral surface reaction is given by $4Fe^{2+} + O_2 + 6H_2O \rightarrow 4FeOOH_{(core)} + 8H^+$. As the protein progressively acquires iron, oxidation/hydrolysis increasingly shifts from a ferroxidase site to a mineral surface based mechanism, decreasing the production of H_2O_2.

Ferritins are a class of intracellular iron storage proteins distributed throughout the plant and animal kingdoms (*1*−*5*). Ferritin is composed of 24 subunits assembled into a nearly spherical hollow structure capable of storing up to 4500 iron atoms in the form of a hydrous ferric oxide mineral core. In mammals, two types of subunits, H and L, with similar sequences and molecular weights are found in varying amounts in ferritins from different tissues (*3, 6*). The presence of both H- and L-subunits in the same protein molecule appears to be biologically favored since, with the exception of serum ferritin, heteropolymers of H- and L-subunits are normally found (*7*). The two types of subunits have complementary roles in iron oxidation and deposition in the protein (*7*−*9*). The H-subunit facilitates the oxidation of Fe(II) to Fe(III), a property attributable to a binuclear iron ferroxidase site located on the interior of protein in the center of the 4 helix bundle of the H-chain (*1, 10, 11*). No corresponding site is found on the L-subunit. The L-chain has a greater inner surface negative charge and appears to provide nucleation sites for the formation of the mineral core (*7*−*9*, *12*).

Kinetic studies of iron oxidation and deposition in horse spleen ferritin (HoSF)[1] and recombinant human H-chain ferritin (HuHF) using electrode oximetry suggest that ferritins have enzymatic activity (*13, 14*). The overall iron oxidation and core formation reaction at small iron/HoSF increments (Fe/protein < 50) is described by reaction 1, in which the dioxygen is reduced to hydrogen peroxide, a process thought to take place at the ferroxidase site (*14, 15*).

$$2Fe^{2+} + O_2 + 4H_2O \rightarrow 2FeOOH_{(core)} + H_2O_2 + 4H^+ \quad (1)$$

However, when the iron/protein increment increases to greater than 200, evidence suggests that the oxidation reaction shifts toward a mineral surface pathway in which the dioxygen is ultimately reduced to H_2O according to the following reactions (*15*).

$$\text{Oxidation:} \quad 4Fe^{2+} + O_2 + 4H^+ \rightarrow 4Fe^{3+} + 2H_2O \quad (2)$$

$$\text{Hydrolysis:} \quad 4Fe^{3+} + 8H_2O \rightarrow 4FeOOH_{(core)} + 12H^+ \quad (3)$$

$$\text{Net:} \quad 4Fe^{2+} + O_2 + 6H_2O \rightarrow 4FeOOH_{(core)} + 8H^+ \quad (4)$$

Reactions 1 and 4 occur on the time scale of tens of seconds to minutes as measured by electrode oximetry (*13,*

† Supported by Grant R37 GM20194 of the National Institute of General Medical Sciences (N.D.C) and the CNR Target Project on Biotechnology (P.A.).

* Author to whom correspondence should be addressed.
‡ University of New Hampshire.
§ Institute San Raffaele.

[1] Abbreviations: HuHF, human H-chain ferritin; HuLF, human L-chain ferritin; HoSF, horse spleen ferritin; Mes, 2-(*N*-morpholino)-ethanesulfonic acid; Mops, 3-(*N*-morpholino)propanesulfonic acid; NTA, nitrilotriacetic acid; SDS−PAGE, sodium dodecyl sulfate−polyacrylamide gel electrophoresis.

S0006-2960(97)03128-0 CCC: $15.00
Published on Web 06/18/1998

14). In the present study, the oxygen electrode response has been reexamined and tested on model reactions, confirming previous findings that electrode oximetry accurately measures the steady-state oxygen uptake kinetics of ferritin (*13*, *14*). Furthermore, instrumentation has been developed which combines electrode oximetry and pH stat to simultaneously monitor both the kinetics of oxygen uptake and the kinetics of Fe(III) hydrolysis. A clear distinction between ferroxidase site and mineral surface processes is seen in both the kinetic and stoichiometric data from the oxygen and pH stat electrodes. The oxidation/hydrolysis reaction involving the dinuclear ferroxidase site prior to transfer of iron to the core is defined for the first time. Moreover, the hydrolysis reaction associated with the migration of iron from the ferroxidase site to the mineral core has now been established. Spectroscopic titration data in conjunction with the observed hydrolysis chemistry suggest that the dinuclear iron center of the ferroxidase site is a μ-oxo-bridged species. The ferroxidase activity of the H-chain homopolymer, HuHF, regenerates relatively slowly at pH 6.5 and 20 °C, but increases significantly at pH 7.0 and 37 °C and is attributed to increased turnover of iron at the ferroxidase site. The presence of L-chain, as in HoSF, facilitates this process, an effect which is also augmented at pH 7.0. In contrast, iron oxidation in holoHoSF containing about 2000 Fe atoms occurs solely by the mineral surface mechanism. These findings further support the idea that naturally occurring heteropolymeric ferritins exhibit enzymatic behavior early in the formation of the incipient core after which iron oxidation and hydrolysis occur directly on the growing mineral surface.

MATERIALS AND METHODS

Cadmium-free horse spleen ferritin was purchased from Boehinger-Mannheim GmbH (Germany) and from Sigma (Sigma Chemical Co., St. Louis, MO). The H-subunit content of HoSF was determined from densitometric scans of SDS−PAGE gels (*6*). Recombinant human H- and L-chain ferritins were prepared as described elsewhere (*16*, *17*). Apoferritins were prepared by reduction with dithionite (*12*). Apoprotein concentrations were determined by the BioRad assay (*18*, *19*) and absorbance at 280 nm (*20*). Ferrous sulfate was from Baker Scientific Inc., and Mes buffer from Research Organics. The enzyme catalase was purchased from Boehinger-Mannheim GmbH (Germany). All other chemicals were reagent grade or purer.

Kinetics of oxygen uptake and hydrolysis were monitored simultaneously in a specially designed 0.48 mL reaction cell fitted with an oxygen microelectrode (MI 730), a customized pH microelectrode, and a Ag/AgCl reference electrode (MI 402), all from Microelectrodes Inc., NH. The cell also contained a NaOH delivery lead from a Radiometer pH stat apparatus consisting of an ABU80 autoburet, a TTT80 titrator, and a PHM82 pH meter (Radiometer Copenhagen, Denmark). A personal computer with an ADA 2000 board (Real Time Devices, Inc.) was used to acquire data from both the oxygen meter and the pH stat system.

To test the response of the oxygen electrode, the electrode was equilibrated in water (21% O_2) and then quickly plunged into a rapidly stirred 100 mM dithionite solution (0% O_2), and the electrode output measured vs time. The electrode response followed first-order kinetics with a half-life of 2.3 s. Similarly, the half-life response of the pH electrode was determined to be 0.8 s (pH value) by quickly changing buffer solutions from pH 7.0 to 4.0.

The accuracy of measured oxygen consumption rates was tested by using the oxidation of 0.1−0.4 mM Fe(II) in a 4 mM NTA, 0.15 M NaCl solution at pH 6.30. A rate law of $d[O_2]/dt = k[FeNTA][O_2]$ was obtained with a k value of 58 M^{-1} s^{-1} at 20 °C which is in reasonable agreement with the published value of 80 M^{-1} s^{-1} at 25 °C (*21*).

The accuracy of measured hydrolysis rates was tested using the pseudo first-order hydrolysis reaction of *tert*-butyl chloride in water. A 0.007 M stock solution of *tert*-butyl chloride in acetone was added to a solution containing 0.1 M Na_2SO_4 at 20 °C. As the reaction proceeded, the pH was maintained at pH 6.5 by autotitration with 5.00 mM NaOH using the pH stat apparatus. A rate constant k of 0.025 ± 0.005 s^{-1} was obtained based on the rate law $d[H^+]/dt = k$[*tert*-butyl chloride]$_0$, which is in good agreement with the published values of 0.020−0.037 s^{-1} (*22*).

Most of the iron oxidation reactions were conducted at pH 6.5 or 7.04 and 20 °C unless otherwise indicated. The oxygen-saturated (21% of atmosphere) and very weakly buffered solution containing 0.5 mM Mes or Mops, 0.15 M NaCl, was added to the reaction cell without an air headspace or trapped air bubbles. The solution was rapidly stirred with a micro spin bar to ensure complete mixing of the added iron and NaOH delivered by the pH stat. The reaction was initiated by the addition of freshly prepared anaerobic 20.0 mM $FeSO_4$ stock solution at pH 3.5. A pH stat proportional band setting of 0.1 was usually employed to prevent overshooting. The oxygen consumption and the proton release rates were recorded as the oxygen percentage decreased and microliters of NaOH delivered, respectively. Kinetics calculations and curve fittings were carried out after data acquisition using the software Origin (Microcal Scientific, Inc.).

The initial rates of iron oxidation measured as oxygen consumption and hydrolysis were obtained from the linear A_1 term of third-order polynomial curve fitted to the experimental data, namely $Y = A_0 + A_1t + A_2t^2 + A_3t^3$ and $dY/dt = A_1 + 2A_2t + 3A_3t^2$ (at $t = 0$, $(dY/dt)_0 = A_1$). Here t is the time in seconds, and Y is either the percent oxygen saturation or the delivered NaOH concentration in the sample solution. The final rate was determined by multiplying A_1 by the saturated oxygen concentration (0.28 mM at 20 °C) divided by 21%. The stoichiometric ratios, Fe(II)/O_2 and H^+/Fe(II), were calculated from the concentrations of O_2 consumed and H^+ produced at the completion of the reaction and from the initial concentration of ferrous sulfate added to the solution. An initial sharp increase in NaOH delivery, mainly due to Fe(II) binding to apoprotein, is subtracted from the data prior to the curve fitting procedure since oxidation is not involved. The free acid in the stock $FeSO_4$ solution (20.0 mM) was determined to be 0.026 H^+/Fe(II) as measured from anaerobic addition of $FeSO_4$ to the 0.15 M NaCl, 0.5 mM Mes, pH 6.5 solution in the absence of protein.

Spectroscopic titration experiments were performed using a Hewlett-Packard (HP 8453) diode array spectrometer. The concentrations of the protein were 2.5 μM for HuHF and 10.0 μM for HoSF in 0.15 M Mes buffer, pH 6.5. For the anaerobic experiment, 1 mL HuHF solution was first added

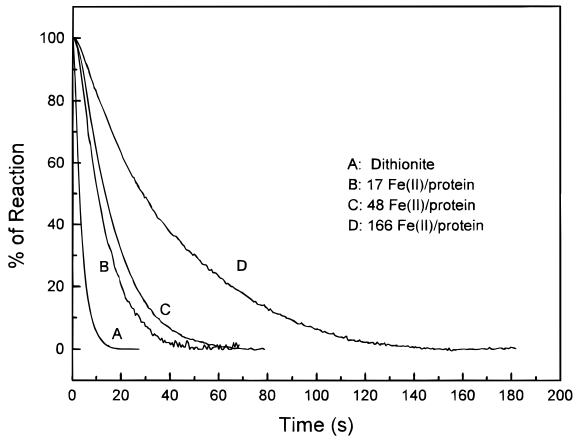

FIGURE 1: Oxygen electrode response (A) between 21% O_2 saturated water and 0% O_2 in 0.1 N $Na_2S_2O_4$ solution, and oxygen consumption curves for (B) 17 Fe(II)/protein, (C) 48 Fe(II)/protein, and (D) 166 Fe(II)/protein solutions. Conditions: [HuHF] = 3.0 μM for (B) and (C), 1.0 μM for (D), $[O_2]_0$ = 0.28 mM, in 0.15 M NaCl and 0.5 mM Mes at pH 6.5 and 20 °C. The half-lives of the response test and the oxygen uptake reactions with 17 Fe, 48 Fe, and 166 Fe/protein are 2.3, 10.2, 13.8, and 30.6 s, respectively.

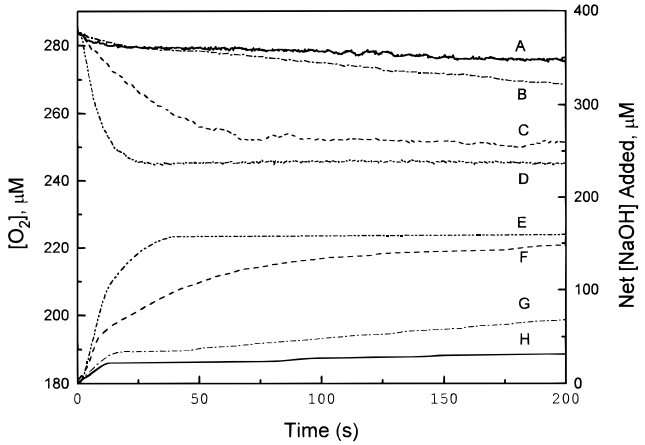

FIGURE 2: Oxygen consumption (A, B, C, D) and proton release (E, F, G, H) versus time for Fe(II) oxidation and hydrolysis in the absence of protein (A, H) and in the presence of HuLF (B, G), HoSF (C, F), and HuHF (D, E). Conditions: [HuLF] = 3 μM, [HoSF] = 3 μM, [HuHF] = 2.5 μM, [Fe(II)] = 150 μM for buffer, HuLF, and HoSF, [Fe(II)] = 83 μM for HuHF, in 0.15 M NaCl and 0.5 mM Mops pH stat titrated with 10.0 mM NaOH at an initial $[O_2]_0$ = 0.28 mM, pH 7.0 and 20 °C.

to a quartz cuvette fitted with a septum and deoxygenated with Ar for 2 h with a micro stir bar placed in the cuvette. Pure protein solutions before Fe(II) addition served as a blank for absorbance measurements. The aerobic titrations were conducted using 1.00 mL of protein and 1.0 μL of Fe(II) for each injection. After each Fe(II) addition, several spectra were taken until the absorbance increased no further, and the final absorbance was taken as the total absorbance.

RESULTS

Oxygen Electrode Response. The oxygen electrode response curve and oxygen consumption curves for Fe(II) oxidation in HuHF are plotted in Figure 1 for comparison. The half-lives for the oxygen uptake in HuHF samples with 17 Fe, 48 Fe, and 166 Fe/protein, are 10.2, 13.8, and 30.6 s, respectively, which are long compared to the 2.3 s half-life for the electrode response. Thus, the response of the electrode is not the limiting factor in the observed kinetics. Nevertheless, kinetics simulations were carried out to quantify the effect of electrode response on the measured value of the initial rates.[2] The results showed that, in the case of the fastest reaction (17 Fe/protein), an electrode response time of $t_{1/2}$ = 2.3 s decreases the measured initial rate by only 9% compared to an electrode with zero response time. We therefore conclude that oxygen uptake kinetics can be reliably measured with the present system. This conclusion is further supported by the data below.

Kinetics of Fe(II) Oxidation and Hydrolysis in Ferritins. Figure 2 shows the oxygen consumption (A, B, C, D) and the corresponding proton release (E, F, G, H) profiles as a function of time for different ferritins. Fe(II) was added to a slightly buffered NaCl solution in the absence of ferritin (A, H) or in the presence of HuLF (B, G), HoSF (C, F), or HuHF (D, E). It can be seen that the Fe(II) oxidation and hydrolysis reactions are facilitated by all the ferritins with reaction rates following the order of HuHF > HoSF > HuLF > buffer, increasing according to the ferritin H chain composition. The similar shapes of the corresponding kinetic curves for both oxygen consumption and proton release indicate that the Fe(II) oxidation and Fe(III) hydrolysis reactions are coupled to one another; namely, oxidation is required for hydrolysis and the processes are concerted or nearly so. We see little proton production from Fe(II) binding to the apoprotein prior to its oxidation, e.g., 0.23 and 0.28 H^+/Fe(II) at pH 6.5 and 7.0, respectively, for Fe(II) added anaerobically in increments of 4 Fe(II)/HoSF in accord with previous observations (*23*).

Stoichiometries of Oxygen Consumption and H^+ Release in HuHF and HoSF. The Fe(II)/O_2 and H^+/Fe(II) stoichiometric ratios measured at completion of the reaction depend on the Fe(II) loading of the protein. To better define the iron oxidation and hydrolysis chemistries of the protein ferroxidase and mineral surface sites and the transition between the two, a careful titration of the apoprotein with Fe(II) was carried out. In these experiments, increasing amounts of Fe(II) were added to a fresh apoprotein solution each time and allowed to react to completion, and the total oxygen consumed and H^+ produced were then measured. Thus, each data point in Figure 3 represents a different sample to which a single addition of Fe(II) was made. For HuHF, a transition point in both the Fe(II)/O_2 and H^+/Fe(II)

[2] The O_2 electrode measurement is described by the following equation:

$$O_2^* \underset{k_{-1}}{\overset{k_1}{\rightleftharpoons}} O_2 \xrightarrow{k} \text{products}$$

where O_2* and O_2 denote oxygen inside and outside the electrode, respectively, k_1 and k_{-1} are the constants for O_2 diffusion across the electrode membrane, and k is the first-order rate constant for oxygen consumption by ferritin. Since the amount of oxygen consumed by the electrode can be ignored relative to the O_2 concentration outside of the electrode membrane, we can write $[O_2] = [O_2]_0\exp(-kt)$ and $d[O_2^*]/dt = k_{-1}[O_2]_0\exp(-kt) - k_1[O_2^*] = k_{-1}[O_2^*]_0\exp(-kt) - k_1[O_2^*]$, where $[O_2^*]_0$ is the initial oxygen concentration inside the electrode and is equal to $[O_2]_0$ at the start of the reaction. Integration yields $[O_2^*] = [O_2^*]_0[(1-K)\exp(-k_1t) + K\exp(-kt)]$, where $K = k_{-1}/(k_1 - k)$. This equation describes the curves in Figure 1. For the electrode used in this work, $k_1 = k_{-1} = 0.30\ s^{-1}$ ($t_{1/2}$ = 2.3 s). With rapid oxygen electrode response ($k_1 = k_{-1} \gg k$), the measured oxygen concentration is simply a first-order decay: $[O_2^*] = [O_2] = [O_2]_0\exp(-kt)$.

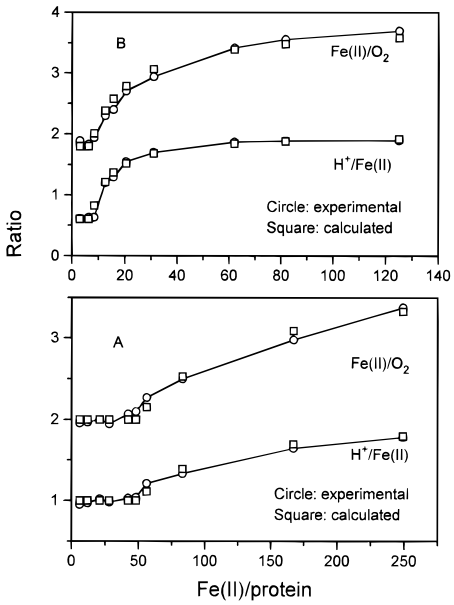

FIGURE 3: Dependence of stoichiometries on Fe(II) loadings in (A) HuHF and (B) HoSF. Conditions: [HuHF] = 1.0−3.0 μM, [HoSF] = 0.25−10.0 μM, in 0.15 M NaCl and 0.5 mM Mops pH stat, pH 7.0 and 20 °C.

curves is revealed near 48 Fe(II)/protein (Figure 3A), which we attribute to the oxidation and hydrolysis of 2 Fe(II) at each of the 24 H-chain ferroxidase sites on the protein. Such a transition is not seen with HuLF (data not shown). Below 48 Fe(II)/protein, the stoichiometric ratios are Fe(II)/O_2 = 1.97 ± 0.03 and H^+/Fe(II) = 0.98 ± 0.04, and correspond to values for chemistry taking place at the ferroxidase site. However, at Fe(II) loadings greater than 48 Fe(II)/protein, the observed Fe(II)/O_2 and H^+/Fe(II) ratios are an average of ferroxidase site and mineral surface stoichiometries. The calculated points in Figure 3A were obtained assuming that the ferroxidase site reaction proceeds with stoichiometries of Fe(II)/O_2 = 2.0 and H^+/Fe(II) = 1.0 and the mineral surface reaction with stoichiometries of 4 Fe(II)/O_2 and 2 H^+/Fe(II) (eq 4), the observed average stoichiometries being given by the following equations:

$$\text{Fe(II)}/O_2 = 4n/[96 + (n - 48)] \qquad \text{For } n > 48$$

$$H^+/\text{Fe(II)} = [48 + 2(n - 48)]/n \qquad \text{For } n > 48$$

Excellent agreement between calculated points and the observed data is obtained (Figure 3A).

Similar transitions are observed for HoSF at 8 Fe(II)/protein (Figure 3B), which we attribute to reaction of two Fe(II) at each of the 4 ferroxidase sites of the protein used in this study which has an average subunit composition H_4L_{20} as determined by SDS−PAGE (see Materials and Methods). However, in this instance ferroxidase site stoichiometries of 1.80 Fe(II)/O_2 and 0.60 H^+/Fe(II) were obtained at Fe(II) loadings below 8 Fe(II)/protein. In other experiments with HoSF, values of Fe(II)/O_2 = 1.8−1.9 and H^+/Fe(II) = 0.6−0.8 were consistently found which are somewhat lower than the theoretical values of 2.0 and 1.0, respectively.[3] At loadings above 8 Fe(II)/protein, the stoichiometric ratios Fe(II)/O_2 and H^+/Fe(II) both increase and approach 4.0 and 2.0, respectively. The calculated points in Figure 3B above 8 Fe(II)/protein assume ferroxidase site values of 0.60 H^+/Fe(II) and 1.80 Fe(II)/O_2, and mineral surface values of 4.0 Fe(II)/O_2 and 2.0 H^+/Fe(II) according to the following equations:

$$H^+/\text{Fe(II)} = [4.8 + 2(n - 8)]/n \qquad \text{For } n > 8$$

$$\text{Fe(II)}/O_2 = 4n/[16.8 + (n - 8)] \qquad \text{For } n > 8$$

Good agreement between calculated and observed points is likewise obtained with HoSF (Figure 3B).

A stoichiometry of Fe(II)/$O_2 \cong 2$ for both HuHF and HoSF implies that H_2O_2 is produced by the ferroxidase site reaction. The addition of catalase to the protein solution prior to the addition of Fe(II) caused the measured stoichiometry to change from 2 Fe(II)/O_2 to 4 Fe(II)/O_2, indicating that H_2O_2 is quantitatively produced in the ferroxidation reaction in accord with previous findings (*15*). If we assume that the observed proton production arises solely from Fe(III) hydrolysis, we may write the ferroxidase site oxidation/hydrolysis reaction for both HuHF and HoSF as

$$2Fe^{2+} + O_2 + 3H_2O \rightarrow [Fe_2O(OH)_2]^{2+} + H_2O_2 + 2H^+ \quad (5)$$

where $[Fe_2O(OH)_2]^{2+}$ represents a postulated hydrolyzed dinuclear Fe(III) center of the ferroxidase site.

From the ferroxidase site reaction in which one proton is produced per iron oxidized (eq 5) and from the previously determined net reaction for core formation via the ferroxidase site (eq 1) (*15*), we can now write the reaction for the transfer of iron from the ferroxidase site to the core, namely:

$$[Fe_2O(OH)_2]^{2+} + H_2O \rightarrow 2FeOOH_{(core)} + 2H^+ \quad (6)$$

After reaction 5 is complete, further hydrolysis then proceeds according to reaction 6, producing one more proton per iron as the mineral core is formed and a vacant ferroxidase site is regenerated (vide infra). This process can be observed directly. For example, when 4 Fe(II) is repeatedly added in 10 min intervals to protein already containing at least 8 Fe/protein, there is an initial rapid phase of proton release (~1 H^+ per Fe^{2+} oxidized) at a rate paralleling O_2 consumption as per the ferroxidase site reaction 5 (data not shown). This first phase is complete within 1 min and is followed by a slower phase of proton production which takes place over a period of about 10 min or so and accounts for one more H^+ per iron as per eq 6. At the end of this period, full ferroxidase activity is again achieved (vide infra).

Spectrophotometric Titrations. UV spectral absorption around 305−330 nm has been traditionally used to monitor core formation in ferritins (e.g., refs *24*, *25*). Absorbances in this spectral region are seen in ribonucleotide reductase, hemerythrin, and a number of model compounds, all of which contain μ-oxo-bridged Fe(III) dimers (*26*, *27*), the inference being that the dinuclear Fe(III) ferroxidase site of ferritin likewise is a μ-oxo-bridged species (*3*, *28*). We therefore

[3] Although Fe(II)/O_2 ratios less than 2.0 imply the production of some O_2^-, the addition of superoxide dismutase had no effect on the oxidation stoichiometry. Fractional values of H^+/Fe(II) can occur when there is a small increase in pK_a of protein functional group(s) upon iron oxidation/binding.

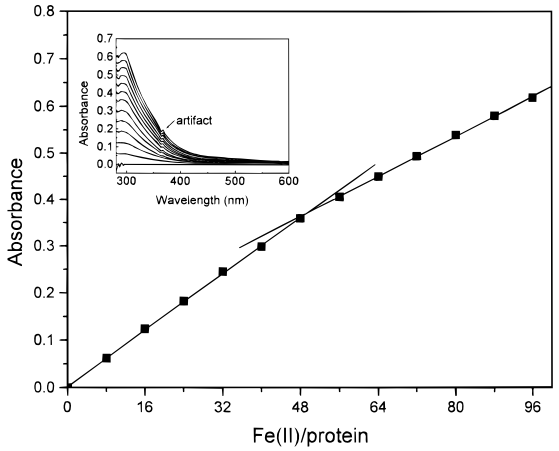

FIGURE 4: Absorbance at 305 nm versus iron loading of HuHF. Conditions: [HuHF] = 2.5 μM in 0.15 M NaCl and 0.15 M Mes buffer at 20 °C, pH 6.5. Inset: Titration spectra for each addition of 8 Fe(II)/protein.

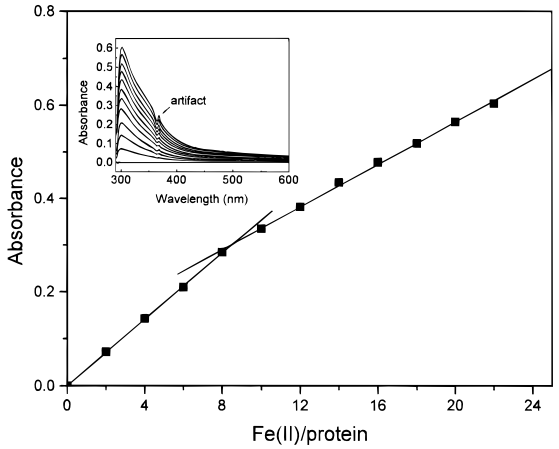

FIGURE 5: Absorbance at 305 nm versus iron loading of HoSF. Conditions: same as in Figure 4 except the [HoSF] = 10.0 μM. Inset: Titration spectra for each addition of 2 Fe(II)/protein.

investigated the origin of this absorbance in ferritin more closely. The anaerobic addition of Fe(II) to either HuHF or HoSF produced no UV absorbance, but upon introduction of air into the solution, a band with a maximum absorbance at 305 nm immediately emerged, demonstrating that the absorbing species in these samples is oxygen related.

Careful aerobic spectrometric titrations of both HuHF and HoSF with Fe(II) were therefore carried out (Figures 4 and 5). Discontinuities in absorbance at 48 Fe(II)/HuHF (Figure 4) and 8 Fe(II)/HoSF (Figure 5) are evident, consistent with the stoichiometries of iron binding at the ferroxidase sites of these proteins. The changes in slope at these stoichiometries suggest that, after saturation of the ferroxidase sites with Fe(III), different oxidation products are formed, namely Fe(III) clusters with smaller molar absorptivity than the dimers. The molar absorptivities of the ferroxidase sites of HuHF and HoSF are 5980 and 7080 M^{-1} cm^{-1} per iron at 305 nm, respectively, and fall in the range of those of other μ-oxo-bridged iron(III) dimers in proteins and model compounds (*26*). The band is assigned to a μ-oxo ligand-to-Fe(III) charge-transfer transition. Thus, we postulate that the hydrolyzed iron of the ferroxidase site is a μ-oxo-bridged binuclear species of formula $[Fe_2O(OH)_2]^{2+}$ rather than a hydrated $[Fe_2(OH)_4]^{2+}$ species. The corresponding molar absorptivities of the μ-oxo-bridged iron(III) clusters formed

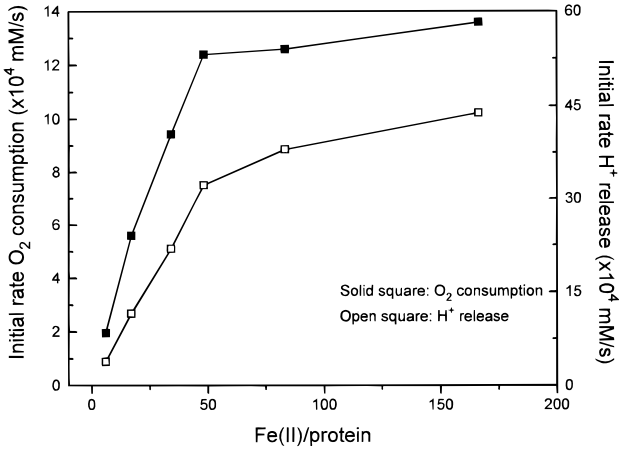

FIGURE 6: Initial rates of oxygen consumption and proton release versus the Fe(II) loadings in HuHF. Conditions: [HuHF] = 3.0 μM except for the 166 Fe(II)/protein sample for which the [HuHF] = 1.0 μM, $[O_2]_0$ = 0.28 mM, in 0.15 M NaCl and 0.5 mM Mes at pH 6.5 and 20 °C.

after the ferroxidase site dimer are 4280 and 4570 M^{-1} cm^{-1} per iron for HuHF and HoSF, respectively.

Initial Rate of Oxygen Consumption and Proton Release in HuHF. The stoichiometries of iron binding, oxidation, and hydrolysis in HuHF are also seen in the kinetics data. Initial rates of oxygen consumption and proton release as a function of Fe(II)/HuHF ratio at pH 6.5 are plotted in Figure 6. Each data point represents a separate apoferritin sample to which a single addition of Fe(II) was made. We attribute the marked fall-off in both the oxidation and hydrolysis curves at about 48 Fe(II)/protein to a transition from a ferroxidase site dominated mechanism to a mineral surface one. Moreover, the initial rates of both oxygen consumption and proton release increase linearly with Fe(II) concentration for Fe(II) loadings up to 48 Fe(II)/protein, indicating that these processes are first-order in iron. Furthermore, below 48 Fe/HuHF the ratio of the initial rates of proton production to oxygen consumption, v_{H^+}/v_{O_2}, is approximately 2:1 in accord with the derived stoichiometry for the ferroxidase reaction (eq 5), further confirming the validity of the use of electrodes to study the kinetics of oxygen consumption and iron hydrolysis in ferritin.

Regeneration of Ferroxidation Activity in HuHF and HoSF. The ability of the ferroxidase site to regenerate its oxidative activity in HuHF and HoSF was determined from the initial rate of oxygen consumption and from the Fe(II)/O_2 stoichiometry ratio measured at completion of the reaction. In these experiments Fe(II) was repeatedly added to the same protein sample at different temperatures (20 or 37 °C), pH (6.5 or 7.0), and time intervals between additions (3, 5, or 10 min). A single Fe(II) addition corresponded to half saturation of the ferroxidase site, i.e., 24 Fe(II)/protein for HuHF and 4 Fe(II)/protein for HoSF. The initial rates, normalized to the initial rate observed for the first injection, versus the number of injections are plotted in Figure 7. For the experiments performed at 20 °C and pH 6.5 and with time intervals about 3 min between injections, the residual activity for the H-chain homopolymer is much lower than for the HoSF (Figure 7). Well after saturation of the ferroxidase site, i.e., the fifth injection, HoSF still retains about 70% of its original oxidation activity compared to only 30% for HuHF. Also in the case of HuHF there is a sharp

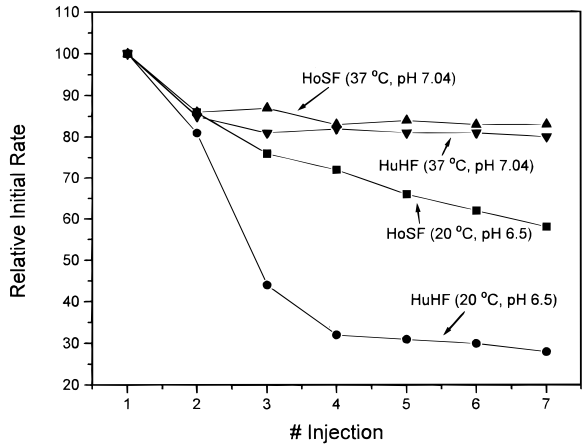

FIGURE 7: Regeneration of oxidation activities in HuHF and HoSF expressed as normalized initial rates. Each injection is half saturation of the ferroxidase site, i.e., 4 Fe(II)/protein for HoSF and 24 Fe(II) for HuHF. (▲) HoSF in 0.15 M NaCl, 0.5 mM Mops, pH 7.04, 37 °C, time intervals between injections of 10 min, (▼) HuHF in 0.15 M NaCl, 0.5 mM Mops, pH 7.04, 37 °C, time intervals between injections of 10 min, (■) HoSF in 0.15 M NaCl, 0.5 mM Mes, pH 6.5, 20 °C, time intervals between injections of 3 min, (●) HuHF in 0.15 M NaCl, 0.5 mM Mes, pH 6.5, 20 °C, time intervals between injections 3 min.

drop in initial rate on the third injection, i.e., right after an iron/protein stoichiometry corresponding to ferroxidase site saturation, but not so for HoSF, a further indication that HoSF is superior in regenerating its oxidation activity under these conditions. However, both proteins regenerate their ferroxidase site activity more completely at the higher pH (7.04) and temperature (37 °C), and at longer time intervals of 10 min between Fe(II) additions as shown by the top two traces in Figure 7. After a drop in the initial rate of about 15% following the second injection, both proteins retained about 85% of their activity in all subsequent injections.

That the observed regeneration of ferroxidase activity corresponds to iron oxidation being restored at the protein ferroxidase site is confirmed by the net $Fe(II)/O_2$ stoichiometry measured at the completion of the reaction (Figure 8). Under most conditions, the amount of Fe(II) oxidized per O_2 consumed increases from 2 $Fe(II)/O_2$ with each injection for both proteins, indicating an increasing involvement of the mineral surface mechanism. Again higher pH and temperature and a longer time interval between iron injections favor oxidation at the ferroxidase site. For example, at pH 7.04, and 37 °C with time interval about 10 min, HoSF completely regenerates its ferroxidase activity as seen by the constant $Fe(II)/O_2$ ratio of 1.8 (Figure 8B, curve c). Under the same conditions, the $Fe(II)/O_2$ ratio for HuHF increases from 1.97 for the first injection to 2.5 for the seventh injection (Figure 8A, curve f), indicating increasing involvement of the mineral core mechanism in the overall reaction. When Fe(II) is added to holoHoSF containing 2000 Fe, an $Fe(II)/O_2$ ratio of 4.0 is obtained; indicating that in the presence of a sizable core, oxidation occurs by the mineral surface mechanism alone (data not shown). Table 1 summarizes for both proteins the percentage of the iron oxidation which proceeds via the ferroxidase site mechanism following the sixth injection of Fe(II) under various conditions.

DISCUSSION

Iron incorporation in ferritin is a multistep process involving the binding and migration of Fe(II) to the ferroxidase site, Fe(II) oxidation, Fe(III) hydrolysis, and finally nucleation and growth of the mineral core. In the present study, iron deposition in HoSF and HuHF has been carefully examined with respect to both iron oxidation and hydrolysis (Figures 2, 3, 6, 7, and 8). The stoichiometric relationships between O_2, H^+, and Fe^{2+}, as well as their changes with the Fe(II)/protein ratio, have provided detailed information on the mechanisms of oxidative deposition of iron in the protein. Specifically, the ferroxidase site reaction 5 prior to core formation has been determined from the stoichiometry measurements (Figure 3) and further verified by kinetic data (Figure 6). We assign the protons produced in reaction 5 to iron(III) hydrolysis at the ferroxidase site since little proton production occurs upon Fe(II) binding to the protein and because Fe(III) complexes are known to have a propensity to undergo partial hydrolysis (*29*, *30*). The X-ray data indicate that the dinuclear iron(III) center is not coordinatively saturated with protein ligands (*3*, *11*) and is therefore expected to be partially hydrolyzed. The presence of a μ-oxo bridge in the ferroxidase site structure seems likely from the spectrometric titration data (Figures 4 and 5) and from previous interpretations of UV and Mössbauer spectral measurements (*12*, *24*, *31*, *32*). A possible structure for the dinuclear iron ferroxidase center in its oxidized and hydrolyzed form, taking into account X-ray structural data (*3*, *4*,

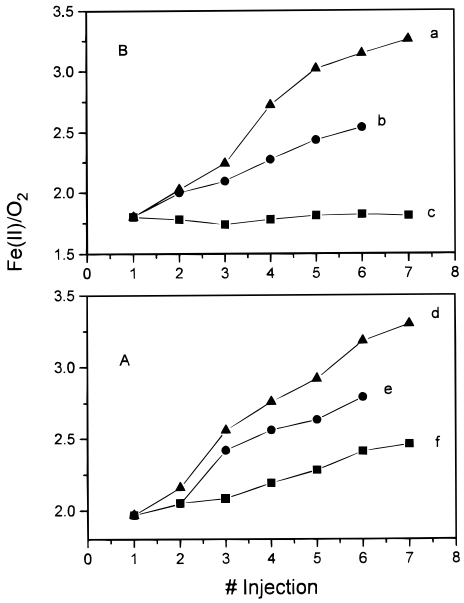

FIGURE 8: $Fe(II)/O_2$ ratio changes in sequential injections of Fe(II) to HuHF (A) and HoSF (B). Conditions: (■) pH 7.04, 37 °C, and 10 min time interval, (●) pH 7.04, 20 °C, and 3 min time interval, (▲) pH 6.5, 20 °C, and 3 min time interval.

Table 1: Percentage of Ferroxidase Site Reaction on the Sixth Fe(II) Injection for HoSF and HuHF[a]

experimental conditions	HoSF (%)	HuHF (%)
pH 6.5, 20 °C, time interval 3 min	43	40
pH 6.5, 37 °C, time interval 3 min	61	ND[b]
pH 7.04, 20 °C, time interval 3 min	73	60
pH 7.04, 20 °C, time interval 5 min	80	ND[b]
pH 7.04, 37 °C, time interval 10 min	100	79

[a] Calculated from the measured stoichiometry according to the following relationship $(Fe(II)/O_2)_{meas} = [2.0X + 4.0(100\text{-}X)]/100$ where X is the percentage of the overall reaction taking place via the ferroxidase site mechanism. Conditions as in Figure 7. [b] Not determined.

Scheme 1

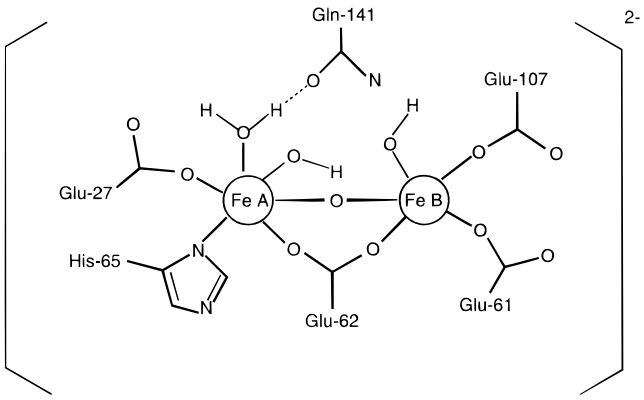

Postulated Ferroxidase Site

11), is therefore postulated in Scheme 1. The distribution of hydroxide on the two iron atoms is not known from the present work, although the postulated structure in Scheme 1 results in a more even distribution of negative charge between the two. A water may be coordinated to Fe_B, making it six-coordinate; however, there is no evidence one way or the other for its presence.

The transfer of Fe(III) from the ferroxidase site to the mineral core, as represented by eq 6, involves the further hydrolysis of iron. UV spectra of the incipient core is obtained which is similar to that of the dimeric ferroxidase site (Figures 4 and 5), as expected since the ferrihydrite core also contains μ-oxo bridges in its structure (*33*, *34*). An intermediate step involving binding of Fe(III) at nucleation sites is not accounted for by eq 6. However, preliminary data (not shown) suggest that proton production is not associated with this step.

Whether the ferroxidase site plays a role in iron oxidation throughout formation of the mineral core or is primarily important in the early stages has been a matter of some interest (*3*, *13*). Previous studies with HoSF reconstituted with cores of various sizes (up to 1200 Fe/protein) have shown that, after the protein had stood for 24 h, oxidation occurred solely by the ferroxidase site pathway when a single further increment of iron(II) (<50 Fe/HoSF) was added to the protein (*13*). The present work demonstrates that, upon repeated additions of iron to the horse and human apoproteins under a variety of conditions, a significant amount of iron (≥40%) is always oxidized via the ferroxidase site mechanism (Figures 7 and 8, Table 1).[4] Under optimal conditions of pH 7.04 and 37 °C, nearly all of the iron(II) is processed by the ferroxidase site in both proteins when there is at least a 10 min delay between Fe(II) additions (Table 1). HoSF is generally superior to HuHF in regenerating the ferroxidase site under a variety of conditions (Figure 7, Table 1), a result consistent with previous studies indicating that the L-chain facilitates mineral formation, presumably due to increased iron turnover at the ferroxidase site in the presence of the L-chain (*14*, *17*, *35*−*38*).

A gradual changeover in reaction mechanism occurs as more iron is repeatedly added to either HoSF or HuHF in the relatively short time intervals of our experiments (3−10 min). As shown in Figure 3, there is a gradual increase in the Fe(II)/O_2 stoichiometry which corresponds to an increase in the amount of iron being oxidized by the mineral surface pathway. Eventually, the changeover to a mineral surface mechanism becomes complete since iron oxidation in holoHoSF occurs with a stoichiometry of 4 Fe(II)/O_2 and a rate about 1/5 that of the ferroxidase site reaction. The lack of a functional ferroxidase site in holoferritin is probably due to blocking of the site by the presence of a sizable mineral core. Ferroxidase site activity is restored upon reductive removal of the iron core (see Materials and Methods), resulting in an apoprotein which can oxidize iron at least five times faster than holoferritin when iron is added in small increments (4 Fe/protein). However, as previously shown, large fluxes of iron into the apoprotein kinetically saturate the ferroxidase site and the bulk of the iron is then oxidized by a mineral surface pathway (*13*).

The ferroxidase site kinetics observed here are consistent with previous findings that the ferritins possess enzymatic activity (*13*, *14*); however, the present study more clearly delineates the transition from the ferroxidase site mechanism to a mineral surface mechanism at iron loading stoichiometries beyond 2 Fe/H-chain (Figures 3, 6, and 7). The results also confirm that the initial rate of oxygen uptake (as opposed to Fe(II) oxidation) is first-order in Fe(II) (*13*) as is also true for proton production (Figure 6). This finding contrasts with the second-order dependence in the rapid UV−visible spectral changes seen in stopped-flow studies of HuHF (*28*, *39*) and also contrasts with stopped-flow and the multiple first-order kinetics observed in rapid-freeze quench Mössbauer studies of iron oxidation in bullfrog H-chain ferritin (*40*, *41*). The rapid phase is slow to recover, requiring up to 24 h before it is observed again upon addition of more iron (*28*, *41*). It perhaps involves a redox component of the protein which is slowly reoxidized by molecular oxygen. Redox centers have been shown to be present on apoHoSF (*42*). Although the connection between the steady-state kinetics investigated here, which are complete in tens of seconds, and the rapid transient kinetics (<1 s) observed by others remains to be firmly established, the present work nevertheless provides new insights into the processes involved in iron deposition in ferritin and has helped to define the chemistries occurring at both the ferroxidase site and the mineral surface and the transition between the two. The bulk of the iron accumulated by ferritin is acquired through the kinetic processes investigated in the present study.

[4] The percentages in Table 1 reflect the fraction of all of the added iron which has been oxidized by the ferroxidase site, whereas the curves in Figure 7 reflect just the initial rates.

REFERENCES

1. Harrison, P. M., Andrews, S. C., Artymiuk, P. J., Ford, G. C., Guest, J. R., Hirzmann, J., Lawson, D. M., Livingstone, J. C., Smith, J. M. A., and Treffry, A. (1991) *Adv. Inorg. Chem. 36*, 449.
2. Proulx-Curry, P. M., and Chasteen, N. D. (1995) *Coord. Chem. Rev. 144*, 347.
3. Harrison, P. M., and Arosio, P. (1996) *Biochim. Biophys. Acta Bio-Energ. 1275*, 161.
4. Harrison, P. M., Hempstead, P. D., Artymiuk, P. J., and Andrews, S. C. (1998) in *Iron Transport and Storage in Microorganisms, Plants, and Animals* (Sigel, A., and Sigel, H., Eds.) pp 435−477, Marcel Dekker, New York.
5. Chasteen, N. D. (1998) in *Iron Transport and Storage in Microorganisms, Plants, and Animals* (Sigel, A., and Sigel, H., Eds.) pp 479−514, Marcel Dekker, New York.

6. Arosio, P., Adelman, T. G., and Drysdale, J. W. (1978) *J. Biol. Chem. 253* (12), 4451.
7. Levi, S., Yewdall, S. J., Harrison, P. M., Santambrogio, P., Cozzi, A., Rovida, E., Albertini, A., and Arosio, P. (1992) *Biochem. J. 288*, 591.
8. Arosio, P., Levi, S., Santambrogio, P., Cozzi, A., Luzzago, A., Cesareni, G., and Albertini, A. (1991) *Curr. Stud. Hematol. Blood Transfus. 58*, 127.
9. Andrews, S. C., Arosio, P., Bottke, W., Briat, J. F., Von Darl, M., Harrison, P. M., Laulhere, J. P., Levi, S., Lobreaux, S., and Yewdall, S. J. (1992) *J. Inorg. Biochem. 47*, 161.
10. Lawson, D. M., Treffry, A., Artymiuk, P. J., Harrison, P. M., Yewdall, S. J., Luzzago, A., Cesareni, G., Levi, S., and Arosio, P. (1989) *FEBS Lett. 254*, 207.
11. Hempstead, P. D., Hudson, A. J., Artymiuk, P. J., Andrews, S. C., Banfield, M. J., Guest, J. R., and Harrison, P. M. (1994) *FEBS Lett. 350*, 258.
12. Bauminger, E. R., Harrison, P. M., Hechel, D., Nowik, I., and Treffry, A. (1991) *Biochim. Biophys. Acta 1118*, 48.
13. Sun, S., and Chasteen, N. D. (1992) *J. Biol. Chem. 267* (35), 25160.
14. Sun, S., Arosio, P., Levi, S., and Chasteen, N. D. (1993) *Biochemistry 32*, 9362.
15. Xu, B., and Chasteen, N. D. (1991) *J. Biol. Chem. 266*, 19965.
16. Treffry, A., Harrison, P. M., Luzzago, A., and Cesareni, G. (1989) *FEBS Lett. 247*, 268.
17. Levi, S., Salfeld, J., Franceschinelli, F., Cozzi, A., Dorner, M. H., and Arosio, P. (1989) *Biochemistry 28*, 5179.
18. Wang, D., and Hanson, G. R. (1995) *J. Magn. Reson. 117*, 1.
19. Sedmack, J. J., and Grossberg, S. E. (1977) *Anal. Biochem. 79*, 544.
20. Heusterspreute, M., and Crichton, R. R. (1981) *FEBS Lett. 129*, 322.
21. Antanaitis, B. C., Brown, R. D., III, Chasteen, N. D., Freedman, J. H., Koenig, S. H., Lilienthal, H. R., Peisach, J., and Brewer, C. F. (1987) *Biochemistry 26*, 7932.
22. Adams, R. E., Betso, S. R., and Carr, P. W. (1994) *Anal. Chem. 48* (13), 1989.
23. Jacobs, D., Watt, G. D., Rankel, R. B., and Papaefthymiou, G. C. (1989) *Biochemistry 28*, 9216.
24. Treffry, A., Hirzmann, J., Yewdall, S. J., and Harrison, P. M. (1992) *FEBS Lett. 302*, 108.
25. Treffry, A., and Harrison, P. M. (1984) *J. Inorg. Biochem. 21*, 9.
26. Que, L., Jr., and True, A. E. (1990) in *Progress in Inorganic Chemistry: Bioinorganic Chemistry* (Lippard, S. J., Ed.) pp 97−200, John Wiley and Sons, New York.
27. Borovic, A. S., Papaefthymiou, V., Taylor, L. F., Anderson, O. P., and Que, L., Jr. (1989) *J. Am. Chem. Soc. 111*, 6183.
28. Treffry, A., Zhao, Z., Quail, M. A., Guest, J. R., and Harrison, P. M. (1995) *Biochemistry 34*, 15204.
29. Schneider, W., and Schwyn, B. (1987) in *Aquatic Surface Chemistry: Chemical Processes at the Particle−Water Interface* (Stumm, W., Ed.) pp 167−196, John Wiley and Sons, Inc.
30. Schneider, W. (1988) *Chimia 42*, 9.
31. Bauminger, E. R., Harrison, P. M., Hechel, D., Hodson, N. W., Nowik, I., Treffry, A., and Yewdall, S. J. (1993) *Biochem. J. 296*, 709.
32. Bauminger, E. R., Harrison, P. M., Nowik, I., and Treffry, A. (1989) *Biochemistry 28*, 5486.
33. Towe, K. M. (1981) *J. Biol. Chem. 256*, 9377.
34. Eggleton, R. A., and Fitzpatrick, R. W. (1988) *Clays Clay Miner. 36* (2), 111.
35. Wade, V. J., Levi, S., Arosio, P., Treffry, A., Harrison, P. M., and Mann, S. (1991) *J. Mol. Biol. 221*, 1443.
36. Santambrogio, P., Levi, S., Cozzi, A., Corsi, B., and Arosio, P. (1996) *Biochem. J. 314*, 139.
37. Santambrogio, P., Levi, S., Cozzi, A., Rovida, E., Albertini, A., and Arosio, P. (1993) *J. Biol. Chem. 268*, 2744.
38. Chasteen, N. D., Sun, S., Levi, S., and Arosio, P. (1994) in *Progress in Iron Research* (Hershko, C., Konijn, A. M., and Aisen, P., Eds.) pp 23−30, Plenum Press, New York.
39. Treffry, A., Zhao, A., Quail, M. A., Guest, J. R., and Harrison, P. M. (1997) *Biochemistry 36*, 432.
40. Pereira, A. S., Tavares, P., Lloyd, S. G., Danger, D., Edmondson, D. E., Theil, E. C., and Huynh, B. H. (1997) *Biochemistry 36*, 7917.
41. Waldo, G. S., and Theil, E. C. (1993) *Biochemistry 32*, 13262.
42. Watt, R. K., Frankel, R. B., and Watt, G. D. (1992) *Biochemistry 31*, 9673.

BI973128A